Interannual variability in the oxygen isotopes of atmospheric CO2 driven by El Nino

Welp, Lisa R.; Keeling, Ralph F.; Meijer, Harro A. J.; Bollenbacher, Alane F.; Piper, Stephen C.; Yoshimura, Kei; Francey, Roger J.; Allison, Colin E.; Wahlen, Martin

1. Comparison with NOAA observations

The NOAA Earth System Research Laboratory Global Monitoring Division (ESRL/GMD) in cooperation with INSTAAR at the University of Colorado, Boulder, has been making high quality measurements of $\delta^{18}O$ of atmospheric CO_2 since the early 1990's and have been making the data publicly available via their website (**http://www.esrl.noaa.gov/gmd/index.html**). Here we compare the longer SIO and CSIRO records presented in the main text with the shorter NOAA records from the same or nearby stations (Figure S1). The NOAA measurements have been screened to include only reliable data based on their own flagging system described online and detrended using the StationFit program in the same way as the SIO and CSIRO records. There are known offsets in the $\delta^{18}O$ scales among the different laboratories, and in 2006 NOAA adjusted their data by +0.82‰ based on laboratory intercomparisons[31,32]. The SIO record measured in the La Jolla laboratory, since approximately 1992, has been adjusted by -0.109‰ to force the scale in agreement with the earlier data measured in the Netherlands laboratory (CIO) and provide continuity to the entire SIO time series[29]. The CIO and CSIRO laboratory scales have historically been close.

The interannual variability of the SIO and NOAA records at Mauna Loa is similar although the magnitude of the variability differs slightly (Figure S1). Both laboratories' measurements have a similar degree of scatter around the long-term spline fit to the data at this station. Large features are also resolved in the SIO New Zealand and NOAA Cape Grim records with a similar degree of scatter. At the South Pole station, however, there are two positive anomalies in 2002 and 2005 in the NOAA data that are not seen in the SIO data. The simple fact that the NOAA record is shorter in length makes it difficult to test the hypothesis we present in this paper in a meaningful way. For that reason, the NOAA data was not included in this analysis.

2. Mass balance formulation of the two-box model

The two-box model is a simplification of atmospheric transport. The intra-hemisphere exchange times with the biosphere that we solve for are slightly shorter than the inter-hemispheric mixing of approximately one year, and slightly longer than intra-hemispheric mixing times of a few months. For that reason, the two-box model represents just enough complexity to describe ^{18}O in CO_2 mixing.

The form of the two-box model follows from consideration of mass balance of the oxygen isotopes of CO_2 in a system in which CO_2 concentration is in steady state and the only forcing of the oxygen isotopes involves gross exchange of oxygen atoms between the atmosphere and surface reservoirs. The mass balance equations have the form:

$$M_N \frac{d\delta_N}{dt} = (\delta_{NB} - \delta_N)F_{NB} + (\delta_{NO} - \delta_N)F_{NO} + (\delta_S - \delta_N)F_{mix} \tag{S1a}$$

$$M_S \frac{d\delta_S}{dt} = (\delta_{SB} - \delta_S)F_{SB} + (\delta_{SO} - \delta_S)F_{SO} + (\delta_N - \delta_S)F_{mix} \tag{S1b}$$

where δ_N and δ_S represent the isotopic composition of atmospheric CO_2 in each hemisphere, δ_{NB} and δ_{SB} represent the $\delta^{18}O$ of CO_2 exchange with the northern and southern hemisphere land biosphere respectively, and δ_{NO} and δ_{SO} are equivalent terms for oceanic exchange. M_N and M_S represent the number of moles of CO_2 in the northern and southern hemispheres, respectively. The F terms are the O-atom exchange fluxes of CO_2 between the atmosphere and the various reservoirs (NB and SB for northern and southern land biota and soils, respectively, NO and SO for northern and southern oceans, respectively, and mix for mixing between the hemispheres).

We allow for interannual variations in δ_N, δ_S and the products $\delta_{NB}F_{NB}$ and $\delta_{SB}F_{SB}$ where the latter account for the forcing of the atmospheric variations associated with interannual climate variations. Specifically, we assume

$$\delta_N = \delta_N{}' + \overline{\delta_N} \tag{S2a}$$

$$\delta_S = \delta_S{}' + \overline{\delta_S} \tag{S2b}$$

$$\delta_{NB}F_{NB} = (\delta_{NB}{}' + \overline{\delta_{NB}})\overline{F_{NB}} \tag{S3a}$$

$$\delta_{SB}F_{SB} = (\delta_{SB}{}' + \overline{\delta_{SB}})\overline{F_{SB}} \tag{S3b}$$

where primes denote interannual perturbations and overbars denote long-term means. All other quantities are assumed constant in time, including isotopic exchange with the ocean (i.e. $\delta_{NO}{}' = \delta_{SO}{}' = 0$). In Eq. S3a and S3b the ENSO forcing is formally accounted for via the quantities $\delta_{NB}{}'$ and $\delta_{SB}{}'$. Substituting Eq. S2 and S3 into Eq. S1 yields

$$\frac{d\delta_N{}'}{dt} = \frac{\delta_{NB}{}'}{\tau_{NB}} - \frac{\delta_N{}'}{\tau_N} + \frac{\left(\delta_S{}' - \delta_N{}'\right)}{\tau_{mix}} \tag{S4a}$$

$$\frac{d\delta_S{}'}{dt} = \frac{\delta_{SB}{}'}{\tau_{SB}} - \frac{\delta_S{}'}{\tau_S} + \frac{\left(\delta_N{}' - \delta_S{}'\right)}{\tau_{mix}} \tag{S4b}$$

where

$$\tau_{NB}{}^{-1} = \frac{\overline{F_{NB}}}{M_N} \tag{S5a}$$

$$\tau_{SB}^{-1} = \frac{\overline{F_{SB}}}{M_S} \tag{S5b}$$

$$\tau_N^{-1} = \frac{\overline{F_{NB}} + \overline{F_{NO}}}{M_N} \tag{S6a}$$

$$\tau_S^{-1} = \frac{\overline{F_{SB}} + \overline{F_{SO}}}{M_S} \tag{S6b}$$

$$\tau_{mix}^{-1} = \frac{\overline{F_{mix}}}{M_N} \tag{S7}$$

and where we have assumed that the time-invariant terms in Eq. S1 satisfy the relevant steady-state relation.

Eq. S4a and S4b are identical to Eq. 1 and 2 in the main text with the substitutions

$$\frac{\delta_{NB}{}'}{\tau_{NB}} = f_N \cdot A \cdot \mathrm{ENSO}'(t - \mathrm{lag}) \tag{S8a}$$

$$\frac{\delta_{SB}{}'}{\tau_{SB}} = f_S \cdot A \cdot \mathrm{ENSO}'(t - \mathrm{lag}) \tag{S8b}$$

which assume that the biospheric forcing component is tied to the ENSO index and $f_S = (1 - f_N)$.

Eq. S8a and S8b assume that the interannual forcing is tied to El Niño events, but there is no further assumption about which regions are impacted. The representation of the forcing in terms of the specific variables $\delta_{NB}{}'$ and τ_{NB}, etc. is effectively arbitrary. For example, the quantity δ_{NB} formally represents the isotopic composition of CO_2 obtained after equilibration with northern land biota and soils, while $\delta_{NB}{}'$ represents the perturbation to δ_{NB} due to interannual El Niño variability. Given that the correlations we observed between $\delta^{18}O$-CO_2 and δ_{ppt} and RH were maximized in the low latitudes, it is perhaps more meaningful to assume that the forcing is concentrated in tropical regions spanning both hemispheres, in which case one can define

$$A \cdot \mathrm{ENSO}'(t - \mathrm{lag}) = \frac{\delta'_{ENSO}\phi}{\tau_{globe}} \tag{S9}$$

where δ'_{ENSO} is the effective perturbation to equilibrium value of CO_2 obtained from the exchange with the impacted tropical regions alone, $\tau_{globe} = 2/(\tau_N^{-1} + \tau_S^{-1})$ is the global turnover time of oxygen atoms in atmospheric CO_2, and ϕ is the fraction of the global

isotopic exchange occurring in the impacted tropical regions. We will show how this parameterization is useful in the next section.

3. Station and ENSO index selection details

We chose to emphasize results from the MLO, SPO and ALT stations in our analysis because these sites have low specific humidity, thus minimizing the possibility that samples were impacted by condensation on the inside of the flasks. Liquid water can potentially exchange oxygen atoms with CO_2, contaminating the $\delta^{18}O$-CO_2[33]. Similar interannual variability at moist tropical sites (e.g. KUM, CHR, SAM), as compared to drier sites, suggests that this contamination effect is small in any case. Data from the CSIRO CGO *in-situ* sampling were included because they are measured by an independent lab using an online drying technique, which is believed to yield high quality $\delta^{18}O$-CO_2 results[14], and extends over a similar time frame. Any potential offsets in calibration standards between SIO and CSIRO data sets are not important in this analysis because we examine the interannual variability, not the long term mean.

The most obvious difference between the SIO and CSIRO data is that the positive anomaly in the early 1990s in the CSIRO CGO record precedes the anomalies in the SIO stations by a couple of years (1991-93 versus 1993-94) (Figure 1). It is possible that interannual variability was artificially induced during the early 1990s when both labs were updating the isotope ratio mass spectrometers used to measure $\delta^{18}O$ and $\delta^{13}C$ of CO_2. The CSIRO lab has addressed this potential uncertainty in their record by assigning larger uncertainty to measurements made between 1991 through 1992[15]. However, because we assigned uncertainty based on the standard deviation of residuals between the monthly mean flask observations and the spline fits, this did not loosen the model-data comparison in the early 1990s. We also conducted a model fit of the MLO and SPO station pair excluding data between 1990 and 1995. Best-fit values for the model parameters were not significantly changed, however, the correlation coefficient for the southern hemisphere fit was greatly reduced to 0.18.

Our selection of the El Niño Precipitation Index (ESPI)[13] as the ENSO proxy was guided by the fact that this yielded the lowest residual error between the data and the model. Other indices tested (multivariate ENSO index, SOI, and various monsoon intensity indices) yielded slightly higher error. A preference for the ESPI index could also be justified based on the *a priori* notion that the main driver involves the hydrological cycle on land.

4. Model results and error analysis

Table S1 summarizes the best-fit values and 1-sigma errors for each of the ENSO forcing model parameters: f_N, A, τ_N, τ_S and lag in Eqs. 1 and 2 using the four different station combinations described in the main text plus a hemispheric mean case using the mean of

MLO and ALT for the northern hemisphere and the mean of SPO and CGO for the southern hemisphere. The fitting statistics are also summarized. For each model run, the correlation coefficient for the fit between the northern hemisphere model (δ_N) and the observed station $\delta^{18}O$ comparison is listed; likewise for the southern hemisphere model (δ_S) and station observations. We attempted to remove the effects of autocorrelation for our statistical analysis from the fits by using the approach of Ebisuzaki et al.[17]. In order to determine the improvement of the model fit caused by true variation with ESPI, we repeated the model fit using 1000 time series that were artificially generated to have the same autocorrelation but with phases randomly different from the ESPI index. The 'p-value' listed in Table S1 is the fraction of these model fitting runs with random drivers that have a correlation better than or equal to the model run using the ESPI index. None of the random driver runs had a better fit than using the MLO-SPO station combination. The worst station combination was the ALT-CGO pair which also had the fewest number of $\delta^{18}O$ observations (i.e. shortest data records) to fit with the model. The fit statistics for the hemispheric mean case were better than the model runs that used CGO alone to represent the southern hemisphere.

5. Scale analysis of the dominant forcing contributors

Our interest here is to make rough estimates of the contribution of various processes to the ENSO forcing of the $\delta^{18}O$-CO_2. As a starting point, we consider a simplified model that treats the atmosphere as a single well-mixed box, in contrast to the two hemispheric boxes we've considered up to this point:

$$M_a \frac{d\delta_a}{dt} = (\delta_B - \delta_a)F_B + (\delta_O - \delta_a)F_O \qquad (S10)$$

where M_a is the total number of moles of CO_2 in the atmosphere ($M_a = M_N + M_S$), δ_a is the global average isotopic composition of the atmosphere, F_B is the gross O-atom exchange flux of with the global land biota and soils ($F_B = F_{NB}+F_{SB}$) and F_O is the flux of with the ocean ($F_O = F_{NO}+F_{SO}$). Likewise δ_B and δ_O are the flux-weighted $\delta^{18}O$ of exchange with the land biota and ocean respectively. The one-box model represents the isotopic exchange fluxes as being proportional to differences from average atmospheric isotopic composition. Although this is not a good approximation for all aspects of the problem, such as the tendency for northern hemisphere atmospheric anomalies to be rapidly damped via exchange with the land surface within the northern hemisphere, the approximation is reasonable for estimating contributions to the interannual isotopic forcing, which we define to be independent of the atmospheric anomalies.

By assumption, the forcing is contained within the term $(\delta_B - \delta_a)F_B$, which we expand based on the generalized treatment of Keeling[34] (Eq. F) but including the incomplete hydration of CO_2 by carbonic anhydrase inside leaves identified by Gillon and Yakir[4].

$$(\delta_B - \delta_a)F_B = F_{out}(\delta_c - \delta_a)\theta_{eq} + F_R(\delta_{soil} + \varepsilon_{soil} - \delta_a - \varepsilon_{leaf}) - F_{NEP}\varepsilon_{leaf} + F_{fire}(\delta_{fire} - \delta_a - \varepsilon_{leaf})$$

(S11)

where

F_{fire} = CO_2 released from biomass burning (Pg CO_2 yr^{-1})

F_{NEP} = Net ecosystem production (Pg CO_2 yr^{-1})

F_{out} = CO_2 flux out of the leaves into the atmosphere (Pg CO_2 yr^{-1})

F_R = CO_2 flux from soil into the atmosphere (Pg CO_2 yr^{-1})

δ_a = δ^{18}O-CO_2 of atmospheric CO_2 (‰)

δ_c = δ^{18}O-CO_2 of CO_2 in equilibrium with leaf water (‰)

δ_{soil} = δ^{18}O-CO_2 of CO_2 in equilibrium with soil water (‰)

ε_{leaf} = fractionation associated with net leaf CO_2 uptake (‰)

ε_{soil} = fractionation for diffusion of CO_2 out of the soil (‰)

θ_{eq} = the extent of isotopic equilibrium of CO_2 with leaf water

Although not explicitly indicated, the terms in Eq. S11 must be integrated over the global land surface to yield the total isotopic exchange. We also define the quantities Δ_e, and κ_c according to

$$\Delta_e = \delta_c - \delta_{soil}$$

(S12)

$$\kappa_c = \frac{F_{out}}{F_{in} - F_{out}}$$

(S13)

where F_{in} is the (gross) flux of CO_2 from the atmosphere into leaves of land biota, Δ_e is the isotopic enrichment of leaf water above δ_{soil} and κ_c = a measure of stomatal conductance. κ_c is equivalent to $C_{cs}/(C_a-C_{cs})$ where C_{cs} is the CO_2 partial pressure in chloroplasts at the site of CO_2 hydration and C_a is the atmospheric CO_2 partial pressure.

Eq. S11 allows for incomplete CO_2 hydration in leaves via two effects: (1) a reduction at the rate at which leaf water equilibrates with the atmosphere, via factor θ_{eq} in first term on right hand side of S11; and (2) a reduction in the isotopic fractionation associated with net uptake by leaves, via the fractionation ε_{leaf}. Eq. S11 is formally equivalent to the treatment of Gillon and Yakir[4] taking

$$\varepsilon_{leaf} = \varepsilon_{sto} \frac{\left(1 + \kappa_c \theta_{eq}\right)}{1 + \kappa_c} \tag{S14}$$

where ε_{sto} is the fractionation associated with diffusion into stomata. Note that, in the limit that $\theta_{eq} \to 0$, Eq. S14 yields, as expected, the Farquhar *et al.*[2] relation for a case with zero enzymatic fractionation.

We now carry out a perturbation analysis on all quantities, representing them as means (overbars) and anomalies (primes), e.g., $F_{out} = \overline{F_{out}} + F'_{out}$. For simplicity, we assume there are no perturbations in ε_{soil} and δ_{fire} while the ecosystem is, on average, in balance with respect to carbon, $\overline{F_{NEP}} = 0$. Applying the perturbation analysis to the definition of κ_c and substituting $F_{in} = F_{out} + F_R + F_{fire} + F_{NEP}$ yields:

$$F_{out}' = \overline{\kappa_c}\left(F_R' + F_{fire}' + F_{NEP}'\right) + \kappa_c'\left(\overline{F_R} + \overline{F_{fire}}\right) \tag{S15}$$

Applying perturbation analysis to Eq. S10 and S11, eliminating F'_{out} by means of Eq. S15, and dropping terms that are constant in time (because these are balanced by steady-state relationships), yields:

$$M_a \frac{d\delta_a'}{dt} = Q_{iso} - \delta_a' F_B - \delta_a' F_O \tag{S16}$$

where $F_B = \overline{\theta_{eq} F_{out}} + \overline{F_R} + \overline{F_{fire}}$ is a measure of the gross exchange of CO_2 with land biota and F_O is gross exchange with the ocean. Q_{iso} represents the overall biospheric isotopic forcing and is given by:

$$Q_{iso} = \tag{S17}$$

$$+\delta_s'\left(\overline{\theta_{eq}} \cdot \overline{F_{out}} + \overline{F_R}\right) \tag{S17.1}$$

$$+\Delta_e' \cdot \overline{\theta_{eq}} \cdot \overline{F_{out}} \tag{S17.2}$$

$$+\kappa_c'\left(\overline{F_R} + \overline{F_{fire}}\right) \cdot \overline{\theta_{eq}}\left(\overline{\delta_{soil}} + \overline{\Delta_e} - \overline{\delta_a}\right) \tag{S17.3}$$

$$-\varepsilon_{leaf}'\left(\overline{F_R} + \overline{F_{fire}}\right) \tag{S17.4}$$

$$+F_R'\left[\overline{\delta_s} + \varepsilon_{soil} - \overline{\varepsilon_{leaf}} - \overline{\delta_a} + \overline{\theta_{eq}}\overline{\kappa_c}\left(\overline{\delta_{soil}} + \overline{\Delta_e} - \overline{\delta_a}\right)\right] \tag{S17.5}$$

$$+\theta_{eq}'\overline{F_{out}}\left(\overline{\delta_{soil}} + \overline{\Delta_e} - \overline{\delta_a}\right) \tag{S17.6}$$

$$-F_{NEP}'\left[\overline{\varepsilon_{leaf}} - \overline{\theta_{eq}}\,\overline{\kappa_c}\left(\overline{\delta_{soil}} + \overline{\Delta_e} - \overline{\delta_a}\right)\right] \tag{S17.7}$$

$$+F_{fire}'\left[\overline{\delta_{fire}} - \overline{\varepsilon_{leaf}} - \overline{\delta_a} + \overline{\theta_{eq}}\,\overline{\kappa_c}\left(\overline{\delta_{soil}} + \overline{\Delta_e} - \overline{\delta_a}\right)\right] \tag{S17.8}$$

Each budget term in Eq. S17 identifies a mechanism through which ENSO climate anomalies can result in a change in δ_a. Eq. S17.1 represents changes in δ_{soil} through both soil respiration and its effect on leaf water and the retroflux of CO_2 out of leaves. A shift in δ_{ppt} during ENSO events is a likely driver. Eq. S17.2 represents changes in leaf water enrichment above soil water. A change in RH can lead to large Δ_e anomalies. Eq. S17.3 represents changes in the C_{cs}/C_a ratio, κ_c, or the retroflux of CO_2 out of leaves back into the atmosphere. Changes in stomatal conductance caused by drought stress can make this term non-zero. Eq. S17.4 represents changes in the diffusive fractionation on net CO_2 uptake by a leaf, which is also influenced by changes in the degree of CO_2 hydration and C_{cs}/C_a via Eq. S14. The terms Eq. S17.2, Eq. S17.3 and Eq. S17.4 are all closely related. Eq. S17.5 represents changes in the flux of CO_2 from the atmosphere through the vegetation/soil system without a change in net CO_2 uptake. (F_R is approximately equal to gross primary production with the difference being $F_{NEP} + F_{fire}$) An increase or decrease in primary production will make this term non-zero. Eq. S17.6 represents a change in the amount of CO_2 that equilibrates with leaf water. A shift in C_3 productivity relative to C_4 makes this term non-zero. Eq. S17.7 represents changes in F_{NEP} or the shift caused by CO_2 sequestration in the vegetation/soil system. We expect this term to be small compared to others. Eq. S17.8 represents changes in fire emissions. We expect this term to be small even though δ_{fire} is quite different from δ_a.

Correspondence can be made to the A parameter in the two-box model fit as

$$A = \frac{Q_{iso}}{\text{ENSO} \cdot M_a} \tag{S18}$$

In Table S2, we estimate the contribution of each term in Eq. S17, during El Niño events, to the scale factor A of ENSO events to δ_a variability through Eq. S18. Individual parameters and the values assigned to each are described in Table S3. Based on the correlation analysis of δ_{ppt} and RH with the ESPI index in Figure 3, we realize that: first, the anomalies are not the same everywhere, and second, the strongest signals are in the tropical regions. Therefore, we weighted the δ_{ppt} and RH anomalies from 20ºN to 20ºS in Eq. S17.1 and S17.2 by only 40% of the total global CO_2 fluxes (ϕ in Eq. S9). From the scale analysis in Table S2, we conclude that δ_{ppt} and RH have the largest influence on $\delta^{18}O$ of atmospheric CO_2 as discussed in the main text.

Our analysis neglected to consider ENSO-related changes in air-sea CO_2 exchange, in stratosphere troposphere exchange, and in diffuse light. Previous work investigating the cause of anomalies in the $\delta^{13}C$ of atmospheric CO_2 during El Niño events concluded that changes in the influence of air-sea gas exchange, including the effects of changing temperature and wind speed, was insignificant[35, 36]. Based on the relative differences in the temperature sensitivity of the equilibrium fractionation factors and the magnitude of

the atmospheric excursions, we estimate changes in the air-sea exchange would have a four-fold smaller effect on the observed ENSO signal in $\delta^{18}O$ of CO_2. Aircraft measurements of $\delta^{18}O$ of CO_2 in the upper troposphere and lowermost stratosphere have shown that the stratospheric influence on tropospheric $\delta^{18}O$ of CO_2 is smaller than measurement uncertainty[16]. Changes in cloud cover and aerosols can affect diffuse light reaching vegetation canopies, which can affect the $\delta^{18}O$ of CO_2 exchanging with the biosphere[6]. At this point we are not in a position to evaluate the relationship between ENSO and diffuse light.

6. Implications for GPP

The global damping time constant (τ_{globe}) can be formally related to global gross primary production (F_{GPP}) as follows: First, τ_{globe} can be divided into contributions from the land biosphere (τ_B), oceans (τ_{ocean}), and direct exchange of atmospheric CO_2 with soil (also known as the soil invasion, τ_{inv}):

$$\frac{1}{\tau_{globe}} = \frac{1}{2\tau_N} + \frac{1}{2\tau_S} = \frac{1}{\tau_B} + \frac{1}{\tau_{ocean}} + \frac{1}{\tau_{inv}} \tag{S19}$$

The contribution from the land biosphere can be further divided via Eq. S16 into the flux of CO_2 out of leaves, from soil respiration and from biomass burning.

$$\frac{1}{\tau_B} = (\theta_{eq}F_{out} + F_R + F_{fire})/M_a \tag{S20}$$

where all quantities here are assumed to represent long-term averages. Combining the definition of GPP

$$F_{GPP} = F_{in} - F_{out} = F_R + F_{fire} + F_{NEP} \approx F_R + F_{fire} \tag{S21}$$

with Eq. S13 and S20 yields

$$F_{GPP} = \frac{M_a/\tau_B}{\theta_{eq}\kappa_c + 1} \tag{S22}$$

or from Eq. S19,

$$F_{GPP} = \frac{M_a\left(1/\tau_{globe} - 1/\tau_{ocean} - 1/\tau_{inv}\right)}{\theta_{eq}\kappa_c + 1} \tag{S23}$$

We assumed M_a/τ_{ocean} = 90 Pg C yr^{-1} from widely used estimates of CO_2 exchange between the ocean and atmosphere[34,37]. We used θ_{eq} = 0.78 (ref. 4) and C_{cs}/C_a = 0.57 (ref. 2) leading to κ_c = 1.33 and τ_{globe} = 1.1 − 1.7 years from our two-box model

fits. Recent work by Cousins *et al.*[38] indicates that θ_{eq} may have been overestimated by the method of Gillon and Yakir[4], so we consider $\theta_{eq} = 0.78$ to be an upper bound. Wingate *et al.*[22] estimated that the molecules of CO_2 equilibrating with soil water (M_a/τ_{inv}) could be as high as 450 Pg C yr^{-1} assuming a high degree of enzymatic catalysis by free carbonic anhydrase in soils. Until this publication however, the influence of soil invasion was thought to play a relatively small role in the turnover of ^{18}O of CO_2. Stern *et al.*[39] estimated the soil invasion flux could be as high as 25% of the global average soil respiration rate, or ~15 Pg C yr^{-1}, much smaller than the recent Wingate *et al.*[22] model case study.

Reconciling our estimate of the turnover time of O atoms in CO_2 with a GPP flux of 120 Pg C yr^{-1} (ref. 7 and 37) requires the soil invasion influence of $M_a/\tau_{inv} = 110$-330 Pg C yr^{-1}. If we use more conservative values for M_a/τ_{inv} of 50-220 Pg C yr^{-1} with our τ_{globe} model-fits, we estimate GPP = 150-175 Pg C yr^{-1}. We consider this GPP estimate to be a 'best guess'. The other large uncertainty in this approach is the global C_{cs}/C_a. In fact, Ciais *et al.*[9] and Cuntz *et al.*[10] used higher values of C_{cs}/C_a of 0.63 and 0.75 respectively. A C_{cs}/C_a value of 0.66 would place our calculation of GPP near 120 Pg C yr^{-1}. However, these ratios of ~0.7 are characteristic of ratios of CO_2 in the intercellular air spaces to CO_2 in the atmosphere (C_i/C_a) of C_3 vegetation[40], and omit two things: 1) the significant contribution of C_4 vegetation to global GPP which have lower C_i/C_a, ~0.4 (ref. 46), and 2) the added resistance of diffusion across the mesophyll which makes C_{cs}/C_a less than C_i/C_a ratios[41]. C_4 plants contribute to approximately 20-25% of global GPP[42]. Cuntz *et al.*[10] also discuss how their biosphere model likely over predicts C_i/C_a in the northern hemisphere because they are non-water-limited.

To summarize, our analysis of the turnover time of O in CO_2 leads to a best guess for terrestrial GPP of 150-175 Pg C yr^{-1} and a lower bound of approximately 120 Pg C yr^{-1}. The lower bound is based on the following considerations of the input parameters in Eq. S23: 1) $C_{cs}/C_a = 0.66$ yielding $\kappa_c = 1.9$ is likely an upper bound and lower values would increase GPP, 2) $\theta_{eq} = 0.78$ is likely an upper bound and lower values would increase GPP, and 3) $M_a/\tau_{inv} = 50$-220 Pg C yr^{-1} is a relatively high case, for which there is little evidence at the moment, and lower values would increase GPP.

7. References

31. Masarie, K. A. *et al.* NOAA/CSIRO Flask Air Intercomparison Experiment: A strategy for directly assessing consistency among atmospheric measurements made by independent laboratories. *J. Geophys. Res.* **106**, 20445-20464, doi:10.1029/2000jd000023 (2001).

32. Allison, C. E. *et al.* What have we learned about stable isotope measurements from the IAEA CLASSIC?, in *Report of the 11th WMO/IAEA meeting of experts on carbon dioxide concentration and related tracer measurement techniques, WMO/GAW Report No. 148*, pp. 17-30 (Geneva, 2003).

33. Gemery, P. A., Trolier, M. & White, J. W. C. Oxygen isotope exchange between carbon dioxide and water following atmospheric sampling using glass flasks. *J. Geophys. Res.* **101**, 14415-14420 (1996).

34. Keeling, R. F. The atmospheric oxygen cycle - the oxygen isotopes of atmospheric CO_2 and O_2 and the O_2/N_2 Ratio. *Rev. Geophys.* **33**, 1253-1262 (1995).

35. Winguth, A. M. E. *et al.* El-Nino-Southern Oscillation related fluctuations of the marine carbon-cycle. *Global Biogeochem. Cycles* **8**, 39-63 (1994).

36. Keeling, C. D. *et al.* A three-dimensional model of atmospheric CO_2 transport based on observed winds: 1. Analysis of observational data, in *Aspects of Climate Variability in the Pacific and the Western Americas*, *Geophys. Monogr. Ser.,* vol 55, edited by D. H. Peterson, pp. 165-236, (AGU, Washington, D. C., 1989).

37. IPCC. *Climate Change 2007-The Physical Science Basis: Contribution of Working Group I to the Fourth Assessment Report of the Intergovernmental Panel on Climate Change* (Cambridge University Press, 2007).

38. Cousins, A. B., Badger, M. R. & von Caemmerer, S. C-4 photosynthetic isotope exchange in NAD-ME- and NADP-ME-type grasses. *J. Exp. Bot.* **59**, 1695-1703, doi:10.1093/jxb/ern001 (2008).

39. Stern, L. A., Amundson, R. & Baisden, W. T. Influence of soils on oxygen isotope ratio of atmospheric CO_2. *Global Biogeochem. Cycles* **15**, 753-759 (2001).

40. Jones, H. G. *Plants and microclimate: A quantitative approach to environmental plant physiology.* p. 168 (Cambridge University Press, 1992).

41. Farquhar, G. D., Oleary, M. H. & Berry, J. A. On the relationship between carbon isotope discrimination and the inter-cellular carbon-dioxide concentration in leaves. *Aust. J. Plant Physiol.* **9**, 121-137 (1982).

42.   Still, C. J., Berry, J. A., Collatz, G. J. & DeFries, R. S.   Global distribution of C-3 and C-4 vegetation: Carbon cycle implications. *Global Biogeochem. Cycles* **17**, 1006, doi: 10.1029/2001GB001807 (2003).

43.   van der Werf, G. R. *et al.* Continental-scale partitioning of fire emissions during the 1997 to 2001 El Niño/La Niña period. *Science* **303**, 73-76 (2004).

44.   Schumacher, M. *et al.* Oxygen isotopic signature of CO_2 from combustion processes. *Atmos. Chem. Phys.* **11**, 1473-1490 (2011).

45.   Qian, H., Joseph, R. & Zeng, N. Response of the terrestrial carbon cycle to the El Niño-Southern Oscillation. *Tellus B* **60B**, 537-550 (2008).

46.   Scholze, M., Kaplan, J. O., Knorr, W. & Heimann, M. Climate and interannual variability of the atmosphere-biosphere (CO2)-C-13 flux. *Geophys. Res. Lett.* **30**, 1097, doi: 10.1029/2002GL015631 (2003).

47.   Winslow, J. C., Hunt, E. R. & Piper, S. C. The influence of seasonal water availability on global C_3 versus C_4 grassland biomass and its implications for climate change research. *Ecological Modelling* **163**, 153-173 (2003).

48.   West, J. B., Sobek, A. & Ehleringer, J. R. A simplified GIS approach to modeling global leaf water isoscapes. PLoS ONE 3, doi:10.1371/journal.pone.0002447 (2008).
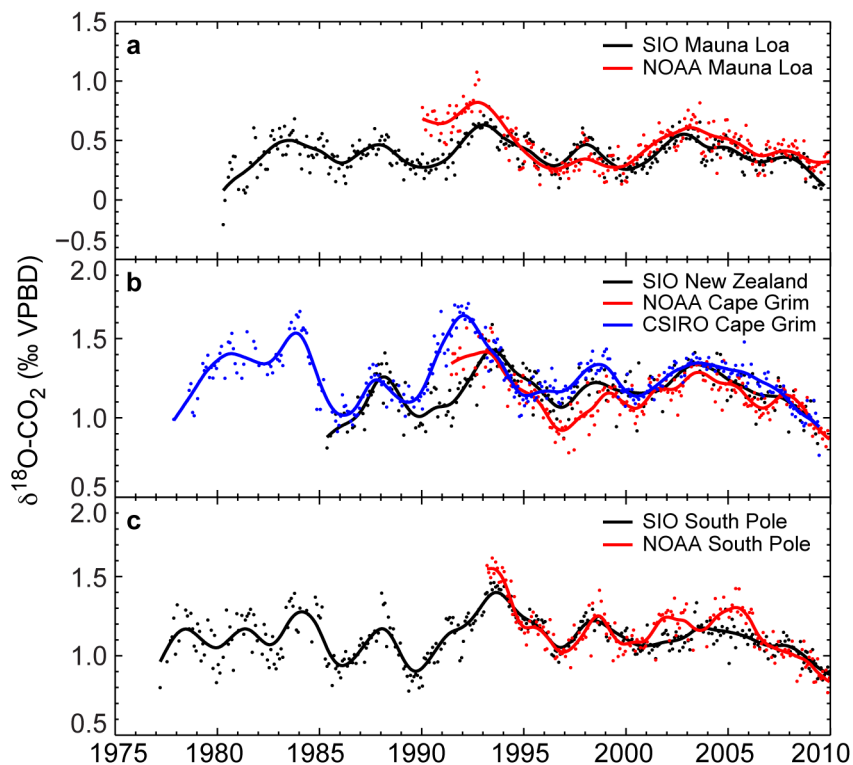
Figure S1: Comparison of SIO δ^{18}O-CO$_2$ with CSIRO and NOAA observations at three stations. **a)** Deseasonalized observations of δ^{18}O of atmospheric CO$_2$ from samples collected at Mauna Loa (MLO) station and analyzed by SIO (black) and NOAA (red). **b)** SIO measurements from New Zealand (NZD) station (black) and NOAA (red) and CSIRO (blue) measurements from Cape Grim (CGO). **c)** SIO measurements from South Pole (SPO) station (black) and NOAA measurements (red).

Table S1: Results, errors, and fit statistics from 2-box model using different combinations of stations for the northern and southern hemispheres. Errors are ± 1-sigma.

Observation Stations	f_N	A	τ_N	τ_S	lag	δ_N model & obs fit statistics		δ_S model & obs fit statistics	
North-South	(unitless)	(‰ ESPI^{-1} yr^{-1})	(yr)	(yr)	(mon)	R	p-value	R	p-value
MLO-SPO[1]	0.76 ± 0.05	0.30 ± 0.03	0.8 ± 0.2	5.0 ± 3.3	0 ± 1	0.499	0.002	0.643	0.000
ALT-SPO[2]	0.49 ± 0.12	0.27 ± 0.04	0.6 ± 0.3	3.8 ± 3.0	1 ± 1	0.314	0.017	0.644	0.003
MLO-CGO[1]	0.62 ± 0.08	0.35 ± 0.04	0.6 ± 0.2	2.6 ± 1.3	-2 ± 1	0.503	0.000	0.520	0.010
ALT-CGO[2]	0.60 ± 0.17	0.30 ± 0.08	0.4 ± 0.3	2.8 ± 2.5	-1 ± 1	0.270	0.025	0.460	0.063
MLO/ALT-SPO/CGO[2]	0.60 ± 0.09	0.28 ± 0.03	0.6 ± 0.2	2.7 ± 1.4	-2 ± 1	0.377	0.012	0.422	0.010

[1]Model fit using data from March 1980 to June 2009.

[2]Model fit using data from May 1985 to June 2009.

Table S2: A scale analysis of contributions of each anomaly term in Eq. S17 to the *A* factor in Eq. S18. The analysis provides a rough estimate of the contribution of ENSO related anomalies in land surface properties to variability in $\delta^{18}O$ of CO_2.

Term in Eq. S17	Land surface property	Contribution to *A* (‰ ESPI^{-1} yr^{-1})
S17.1	δ_{soil} response to δ_{ppt}	0.24[a]
S17.2	Δ_e response to RH	0.16[a]
S17.3	κ_c or C_{cs}/C_a response to drought	0.05
S17.4	ε_{leaf} through κ_c and θ_{eq}	0.00
S17.5	F_R	-0.01
S17.6	θ_{eq} response to C_3/C_4 fraction	-0.01
S17.7	F_{NEP}	-0.02
S17.8	F_{fire}	-0.06
S18	*A*	0.36[b]

[a]Assumes δ_{ppt} and RH anomalies occur in the tropics only and influence 40% of the global terrestrial CO_2 fluxes.

[b]Compare to box model result of *A* = 0.27 to 0.35‰ ESPI^{-1} yr^{-1}.

Table S3: Flux and isotope values used in estimating contributions to Q_{iso} and A. Values listed are global unless indicated otherwise.

Parameter	Description	Estimate	Units
C_a	CO_2 in atmosphere	355	ppm
C_{cs}	CO_2 in chloroplasts	202[a]	ppm
$\dfrac{C_{cs}}{C_a}$	CO_2 ratio between chloroplasts and atmosphere	0.57[2,4]	unitless
$\overline{F_{fire}}$	Mean global fire emissions	3.48[43]	Pg CO_2 yr^{-1}
F_{fire}'	ENSO global fire anomalies	2.16[43]	Pg CO_2 ESPI^{-1} yr^{-1}
$\overline{F_{GPP}}$	Mean gross primary production (GPP)	120.0[7,37]	Pg CO_2 yr^{-1}
F_{GPP}'	GPP anomaly	-0.99[b]	Pg CO_2 ESPI^{-1} yr^{-1}
$\overline{F_{in}}$	Mean flux into leaves	282.6[c]	Pg CO_2 yr^{-1}
$\overline{F_{NEP}}$	Mean net ecosystem production (NEP)	0[d]	Pg CO_2 yr^{-1}
F_{NEP}'	NEP anomaly	-1.68[e]	Pg CO_2 ESPI^{-1} yr^{-1}
$\overline{F_{out}}$	Mean flux out of leaves	159.1[f]	Pg CO_2 yr^{-1}
F_{out}'	Flux out of leaves anomaly	-16.0[g]	Pg CO_2 ESPI^{-1} yr^{-1}
$\overline{F_R}$	Mean ecosystem respiration	120.0[d]	Pg CO_2 yr^{-1}
F_R'	Soil respiration anomaly	0.69[h]	Pg CO_2 ESPI^{-1} yr^{-1}
M_a	Moles of CO_2 in the atmosphere	779.6	Pg CO_2
$\overline{\delta_a}$	Mean $\delta^{18}O$ of atmospheric CO_2	0[i]	‰ VSMOW
δ_a'	δ_a anomaly	0.1[i]	‰ ESPI^{-1}
δ_{fire}	$\delta^{18}O$ of fire CO_2 emissions	-28[44]	‰ VSMOW
$\overline{\delta_{soil}}$	Mean $\delta^{18}O$ of soil CO_2	-7[j]	‰ VSMOW

$\delta_{soil}{}'$	δ_{soil} anomaly	1.9[k]	‰ ESPI^{-1}
$\overline{\varepsilon_{leaf}}$	$\varepsilon_{leaf} = \varepsilon_{sto}\dfrac{\left(1+\kappa_c\theta_{eq}\right)}{1+\kappa_c}$	-6.5	‰
$\varepsilon_{leaf}{}'$	ε_{leaf} anomaly	0.0	‰ ESPI^{-1}
$\overline{\varepsilon_{soil}}$	Mean soil fractionation	-7.2[10]	‰
$\overline{\varepsilon_{sto}}$	Mean stomatal fractionation	-7.4[10]	‰
$\overline{\kappa_c}$	Mean $F_{out}/\left(F_{in}-F_{out}\right)$	1.33	Unitless
$\kappa_c{}'$	$F_{out}/\left(F_{in}-F_{out}\right)$ anomaly	-0.40[l]	ESPI^{-1}
$\overline{\theta_{eq}}$	Fraction of carbonic anhydrase equilibration	0.78[4]	Unitless
$\theta_{eq}{}'$	θ_{eq} anomaly	-0.04[m]	Unitless
$\overline{\Delta_e}$	Mean leaf enrichment above soil	8[n]	‰
$\Delta_e{}'$	Leaf enrichment above soil anomaly	2.5[o]	‰ ESPI^{-1}

[a]Calculated using $C_{cs} = C_a \cdot \dfrac{C_{cs}}{C_a}$

[b]Estimated from global sensitivity of net primary production to ENSO[45].

[c]Calculated using $\overline{F}_{in} = \overline{F}_{out} + \overline{F}_{GPP}$.

[d]Assuming the global carbon cycle is at steady state.

[e]Calculated using $F_{NEP}{}' = F_{GPP}{}' - F_R{}'$.

[f]Calculated using $\overline{F}_{out} = \overline{\kappa_c}\cdot \overline{F}_{GPP}$.

[g]Calculated using $F_{out}{}' = \overline{\kappa_c}\cdot F_{GPP}{}'$.

[h]Estimated from global sensitivity of heterotrophic respiration to ENSO[45].

[i]From observations on the Vienna Standard Mean Ocean Water (VSMOW) $\delta^{18}O$ scale.

[j]Estimated from δ_{ppt} in IsoGSM[14]. NPP-weighted and precipitation amount-weighted annual mean from 20°S to 20°N.

[k]Anomalies in the $\delta^{18}O$ of precipitation range from 1.5 – 4.5‰ ESPI^{-1} for the 1998 El Niño event based on published observations[23,24]. This value is from ENSO anomalies of NPP-weighted and precipitation amount-weighted δ_{ppt} from 20°S to 20°N generated from IsoGSM[14].

[l]Estimated from modelled interannual variability of global mean leaf ^{13}C fractionation[46] and assuming all land biota uses the C$_3$ photosynthetic pathway to calculate a change in C_{cs}/C_a.

[m]Assumes the C$_3$ fraction is reduced from 75% to 65% of global productivity[47].

[n]Estimated from West et al (2008)[48].

[o]Based on a 5% decrease in RH, consistent with observations compiled by the Hadley CRU[27]. Conversion from RH to Δ_e assumes a 15‰ offset between water vapor and plant water and that stomatal diffusion dominates the kinetic isotope fractionation.